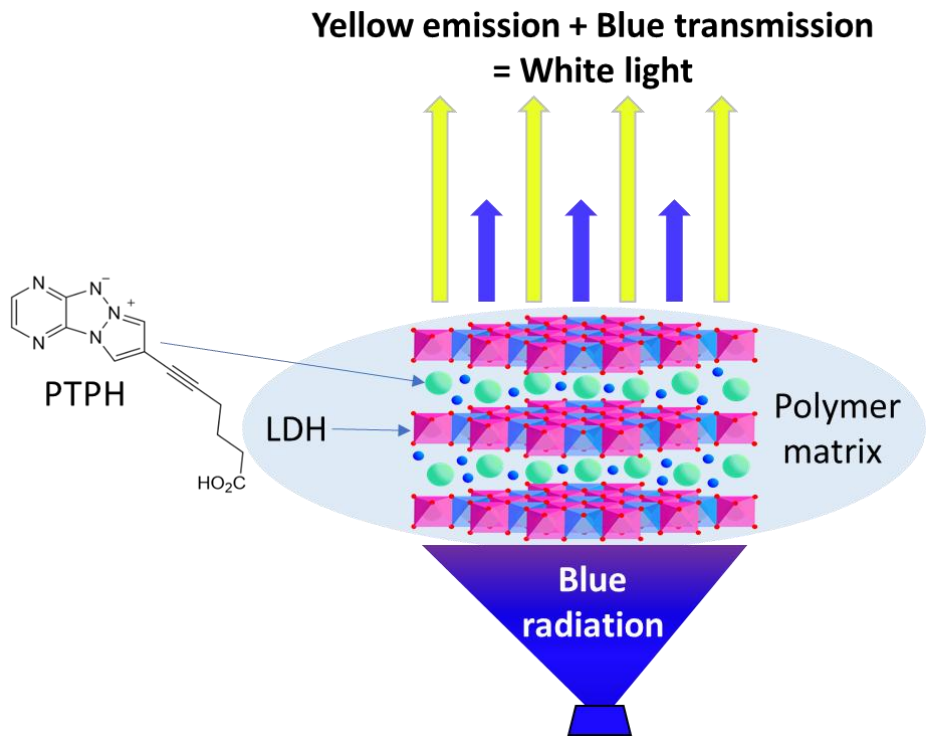
Luminescent N-heterocycles based molecular backbone interleaved into LDH and polymer: for an extensive study

Paul Legentil[a], Geneviève Chadeyron[a], Sandrine Therias[a], Nicolas Chopin[b], Doina Sirbu[b], Franck Suzenet[b], Fabrice Leroux[a,*]

[a]Université Clermont Auvergne, Institut de Chimie de Clermont-Ferrand, UMR CNRS 6296, BP 10448, F-63000 Clermont-Ferrand, France

[b]Université d'Orléans, Institut de Chimie Organique et Analytique - ICOA UMR CNRS 7311, Rue de Chartres, F-45100 Orléans, France

Graphical Abstract



Highlights

- Pyrazino-1,3a,6a-triazapentalene dye type structure was intercalated into LDH by co-precipitation method
- Absolute photoluminescent quantum yields of pristine dye and LDH nanohybrid were compared
- Luminescent composite films were prepared with the LDH nanohybrid filler
- Optical properties of the composite films were characterized for potential lighting devices

Keywords

Layered double hydroxides; Dye; Intercalation; Fluorescence; Composite films.

Abstract

A pyrazino-1,3a,6a-triazapentalene dye-based molecule was intercalated by direct co-precipitation method into the galleries of negatively charged layered double hydroxide (LDH) to form a new luminescent LDH filler. The materials of cation composition Zn/Al = 2 lead to well-defined organic inorganic assemblies. The structure of the hybrid materials was characterized by X-ray diffraction (XRD), Fourier-transform infrared spectra (FTIR) and UV-visible spectra. Optical properties of the materials, at both solid state and slurry state, were also recorded and absolute photoluminescent quantum yields (PLQY) were determined showing that the nanohybrid LDH slurry exhibited higher luminescence properties under UV excitation than the corresponding LDH powder. LDH fillers were used to prepare composite films by dispersion in both hydrophobic or hydrophilic polymer matrix such as poly(dimethyl siloxane) (PDMS) and poly(ethylene oxide) (PEO), respectively. Composite films were

characterized by Small Angle X-ray Scattering (SAXS) and PLQY were recorded in order to compare the behaviour of the nanohybrid LDH filler in both polymer matrices. It was found that the aggregation of particles is still observed by SAXS.

1. Introduction

It is a long-time tradition to use/mix clay minerals with dye molecules, this in particular for coloring used in Egyptian, Maya time, as beautifully exemplified with the famous «blue Maya» as well as for the dye immobilization for water treatment. Both domains were extensively covered with book chapters and reviews(Schoonheydt et al., 2018; Sen, 2017) and are beyond the scope of the present study focusing on advanced sustainable development in lighting devices.

It is known that optical properties may inform on the location and accommodation of the guest organic molecule into or onto the clay mineral as recently reported for laponite and fluorescent dye Safranine simply aggregated or built as Langmuir-Blodgett film (Saha et al., 2017).

As far as clay mineral and organic dye molecule are concerned, polymer may also play a role in dispersion the aggregated assembly as in polyamide fibers for clothes application using montmorillonite (Mmt) (Almasian et al., 2019) or layered double hydroxide (LDH) with azo-dye (Hajibeygi and Omidi-Ghallemohamadi, 2017). Interesting work is also focused on very specific application as those regarding active food packaging polymer, where fluorescent hemicyanine dye-modified Mmt is solvent cast with chitosan to yield bio-nanocomposite films (Mekhzoum et al., 2016).

Concerning LDH, their structure is referred to the natural hydrotalcite mineral, and described with the ideal formula, $[M^{II}_{1-x}M^{III}_{x}(OH)_2]\ [A^{m-}_{x/m}\cdot nH_2O]$, where M^{II} and M^{III} are metal cations,

A^{m-} the interlayered anions, the x value determines the charge density of the LDH and n mol of water molecules per formula weight are also located. Indeed, the isomorphic substitution of M^{II} with M^{III} cations in the brucite-like sheet gives rise to positive electrical charges balanced by exchangeable anions (A^{m-}) leading to the well-known anion exchange/uptake LDH ability.

To date, pioneer works conducted by the group of U. Costantino were at first performed to better understand the host / guest interaction and sometimes to address the location of the organic dye, adsorption versus intercalation by scrutinizing the emission fluorescence and the associated emitting state energy coming from the possible interactions between the excited species of the dye molecule and the neighboring unexcited LDH host structure. This was exemplified with azoic dye methyl orange (MO) into LDH (Zn_2Al cation composition) for which the fluorescence of MO interleaved into LDH was found close to MO itself but shifted at higher energies (Costantino et al., 1999), with the xanthene dye fluorescein surface-immobilized or intercalated into LDH (Zn_2Al), where a dual approach using computer modeling and diffuse reflectance experiments helped in describing guest arrangement (Costantino et al., 2000). Their approach was extended to phenolphthalein Zn_2Al hybrid materials for which space-resolved fluorescence imaged the dyes distribution and their interactions with LDH platelets (Latterini et al., 2002), to a series of chromophores, coumarin-3-carboxylic acid (3-CCA), 9-anthracenecarboxylic acid (9-ACA), 4-benzoylbenzoic acid (4-BBA) and 2-naphthalenesulfonic acid (2-NSA) (Aloisi et al., 2002), as well as covering the emerging aspect of fluorescent filler mostly for hydrophobic polymers with anti-microbial and photo-catalytic applications (Costantino et al., 2013) or simply for mechanical reinforcement (Marangoni et al., 2008).

After this gain in understanding the interaction between LDH and organic dye molecules, more recent study focus merely on applicative properties such as emphasizing on the tunable photoluminescent film using both fluorescein (FLU) and 1-heptanesulfonic acid sodium (HES) / Zn2Al hybrid materials for the electro-catalysis of dopamine (Shi et al., 2010). A step further concerns multicolor light-emitting ultrathin films that were built from Mg_2Al LDH hosting photo-functional anions such as bis(N-methylacridinium)@polyvinylsulfonate ion pairs and derivatives of poly(p-phenylene), poly(phenylenevinylene), and poly(thiophene) showing a well-defined multicolor polarized fluorescence in association to high polarization anisotropy thus making them of interest in light displays and optoelectronic devices (Yan et al., 2011). In the same vein, flexible and robust free-standing films including LDH platelets disposed between poly(vinyl alcohol) (PVA) and a styrylbiphenyl derivative (BTBS) via layer-by-layer (LBL) were found to exhibit luminescent anisotropy (Dou et al., 2013).

Again, facing new concerns for possible development of optical devices such as to be economic, environmental friendly, rare-earth-free, and to address the life cycle assessment and shelf-life and durability of use, all these prompt us to further study hybrid pigments.

These last years, a lot of interest has been carried out to design organic molecules with optical properties for sustainable alternatives of inorganic luminophores, usually composed with rare-earth elements. A lot of organic molecules exhibit very high luminescence property such as N-Heterocyclic compounds and find applications in wide range such as lighting devices (Weber et al., 2015; Zhang et al., 2008), cell imaging sensors (Gogoi and Sen Sarma, 2015; Mahajan et al., 2019; Volpi et al., 2018) or even dye-sensitized solar cells (Lu et al., 2018; Wu et al., 2019). Particularly, pyrazino-1,3a,6a-triazapentalene type organic backbone

has been identified and substituents are possibly attached to tune the optical properties (antenna effect, shift of the absorption/emission spectra) (Sirbu et al., 2019). In terms of tethering to any host structure, such substituents are the functional groups. Indeed, many researches have proven that both the alkyl chain length and the nature of functional groups could subtly and significantly impact the intermolecular interactions and molecular packing and consequently the optical properties of the dye at solid state or in concentrated solutions (Davis et al., 2008; Kumar et al., 2014). The present study is focus on a dye with a pyrazino-1,3a,6a-triazapentalene based molecular backbone and 5-hexynoic acid as substituent, this dye hereafter called compound “PTPH” in the following. The functionalized antenna of PTPH allows its intercalation within a LDH matrix thanks to the bonds occurring between the hydroxyl layers and the carboxylic acid function. Other substituents are also possible such as formic acid and benzoic acid but the PTPH is the only one which presents luminescence property under solid state. Organic molecules at solid state exhibiting luminescence are very rare. Usual dyes such as fluorescein, eosin or rhodamine form aggregates at solid state responsible of the quenching of luminescence (De et al., 2005; Math et al., 2006).

Thus, the dye PTPH has been incorporated into a Zn_2Al LDH matrix by one pot coprecipitation method. The nanohybrid LDH-PTPH was characterised by X-Ray diffraction and FT-IR spectroscopy. The photophysical properties of the pristine dye PTPH and hybrid LDH-PTPH are also scrutinized by UV–visible absorption and fluorescence emission as well as by recording the absolute photoluminescence quantum yield (PLQY). Consequently, composite thin films are prepared by dispersing the LDH-PTPH filler into silicon-type polymer matrix or poly(ethylene oxide). The photophysical properties of the resulting films are also determined in correlation with their morphology analysed by SAXS.

2. Materials and Methods

2.1. Chemicals

The reagents $Zn(NO_3)_2$.$6H_2O$ (purity 99.9+%), $Al(NO_3)_3$.$9H_2O$ (purity 99.9+%) and NaOH (97%) were obtained from Sigma Aldrich. The two-component silicon polymer, Bluesil RTV 141 part A and part B, were supplied by Elkem. The poly(ethylene oxide) (Mw 100,000 $g.mol^{-1}$) was supplied by Scientific Polymer Products.

2.2. Synthesis of PTPH

The N-heterocycles dye called PTPH was synthetized starting from the recently reported bromo derivative **1** (Sirbu et al., 2019). For this purpose, compound **1** was first engaged in a Sonogashira cross-coupling reaction with the methyl-5-hexynoate. The resulting ester **2** was then hydrolysed under basic conditions to afford the desired PTPH (Figure 1).

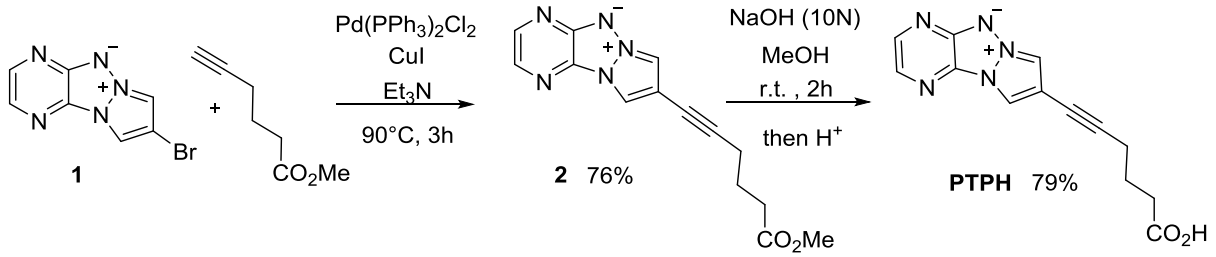


Figure 1 : Synthesis of PTPH

2.3. Synthesis of dye co-intercalated in Zn_2AL LDH

The hybrid layered double hydroxide phase, Zn_2Al–Dye, was prepared by the co-precipitation method. The synthesis of $[Zn_2Al_1(OH)_6]^+[NO_3^-]_{1-x}[PTPH^-]_x \cdot mH_2O$, where $PTPH^-$ is the anionic dye, was performed using the target dye in 50 mL of deionized water. 50 mL of an aqueous solution of Zn^{2+} (1.6 mmol) and Al^{+3} (0.8 mmol) was added dropwise during 3 hours under magnetic stirring. For instance, to prepare the sample LDH-PTPH $[Zn_2Al_1(OH)_6]^+[NO_3^-]_{0.60}[PTPH^-]_{0.4} \cdot mH_2O$, 0.32 mmol of the dye was used. The pH was maintained at 9 by adding

145 0.25 M NaOH during all the addition process. The co-precipitation was performed under
146 nitrogen at 20°C. The mixture was centrifuged at 5 000 rpm during 10 minutes; the
147 sedimented solid on the bottom of the flask was washed several times with deionized water
148 until to obtain a clear and transparent supernatant. A paste was recovered and stored at
149 5°C. A small amount was dried over night at room temperature to obtain a powder for
150 further characterizations and to determine the proportion of the dry extract as well as the
151 uptake of PTPH in LDH-(NO_3^-/$PTPH^-$).

152 ## 2.4. Fabrications of composites thin film Silicon/LDH

153 The LDH hybrid powder was used to elaborate the polymer/hybrid material composite with
154 different loadings. The two-component silicone polymer (silicone Bluesil-RTV 141 A&B) was
155 composed of a viscous liquid called part A cured by polyaddition reaction with a catalyser,
156 part B. The silicone film was prepared following the process: a mixture of the part A and 10
157 phr of part B was prepared, homogenised with mechanical mixer (Planetary Centrifugal
158 vacuum Mixer "Thinky Mixer") during 10 minutes at 500 rpm then pressed in a three rolls
159 mill Exakt 80E. Next, the final composite film was prepared by casting onto a Teflon surface
160 using an Elcometer 4340 automatic film applicator. The blade knife height was fixed at 200
161 µm and the casting speed was 30 mm/s. This two-component silicone polymer was cured at
162 80°C for 2 hours. The film thickness was measured using an Elcometer 456 coating thickness
163 gauge.

164 ## 2.5. Fabrications of composites thin film PEO/LDH

165 The LDH hybrid paste obtained after the last cleaning of LDH-PTPH synthesis was used to
166 elaborate the polymer/hybrid material composite. Hydrophilic poly(ethylene oxide) (PEO)
167 with Mw = 100,000 $g.mol^{-1}$ was used. 1.0 g of PEO powder was dispersed into 10 mL of

deionized water under magnetic stirring during 2 hours. 0.4 g of the LDH-PTPH paste was added to 5.0 g of the previous mixture and then homogenised during 1 hour. The final mixture was poured directly onto a Teflon surface and dried overnight to obtain the composite film PEO-LDH-PTPH.

2.6. Techniques of characterization

2.6.1. X-ray diffraction

LDH powders were characterised by X-Ray Diffraction, the patterns were measured with a Philips X-Pert Pro diffractometer operating with Cu-Kα radiation (λ=1.5418 Å). The data were collected in a 2θ range from 5° to 70° with a step size of 1°/min.

2.6.2. SAXS

Small Angle X-ray Scattering (SAXS) experiments were performed on an Empyrean Panalytical equipment with a ScatterX78 using a θ/θ goniometer and Cu anode (45 kV and 40 mA). An elliptic W/Si focusing X-ray mirror for Cu radiation was used, and divergence fixed slit of 1/32 °. The distance form incident beam to sample was 140 mm. The detector GaliPIX3D was at a distance of 240 mm from the sample. SAXS curves were recorded in continuous scan mode. The background (no sample) was removed in each case.

2.6.3. Fourier transformed-infrared spectroscopy

The infrared spectra were recorded with a Nicolet 5700-FTIR spectrometer with Omnic software. Spectra were obtained using a summation of 32 scans and a resolution of 4 cm^{-1}. Powders of LDH and fluorescein were studied by using the KBr pellet technique.

2.6.4. UV-Visible absorption

The UV–visible absorption spectra of the samples were recorded in the wavelength range of 200 to 800 nm with a UV–vis spectrophotometer (SP-3000 Plus) equipped with an integrating sphere with UV-Probe software.

2.6.5. Luminescence

Quantum yields efficiencies were measured using an integrating sphere C9920−02G PL-QY measurement system from Hamamatsu Photonics. The setup consisted of a 150 W monochromatized Xe lamp, an integrating sphere (Spectralon coating, ⌀= 3.3 in.) and a high sensibility CCD camera. Excitation and blue-excited emission spectra were recorded with a Jobin-Yvon set-up consisting of a Xe lamp operating at 400 W coupled with two monochromators (Triax 550 and Triax 180) and a cryogenically cold charge coupled device (CCD) camera (Jobin–Yvon Symphony LN2 series) for emission spectra and Hamamatsu 980 photomultiplicator for excitation ones. Excitation spectra were corrected for instrument response and Xe lamp intensity using sodium salicylate. The resolution of the system was better than 0.1 nm in both emission and excitation configurations. Luminescence decays were recorded using a second-harmonic generation on a pulsed Nd:YAG OPO Ekspla NT342A laser (3–5 ns pulse duration, 10 Hz, 5 cm^{-1} line width, 0.3 mJ - 20 mJ in the UV-blue). The emitted photons were detected at right angle from the excitation and analysed through Edinburgh FLS980 spectrometer (Czerny-Turner monochromator, 300 mm focal length, 1200 groove mm^{-1} grating and minimum band-pass of 0.1 nm) equipped with Hamamatsu R928P PMT (200–850 nm range).

2.6.6. Scanning electron microscopy (SEM)

Scanning electron microscopy was performed using a ZEISS Supra 55 VP scanning electron microscope in high vacuum, at 20 kV using a back-scatter electron detector (QBSD).

3. Results and Discussion

3.1. Characterisation of the pristine dyes and the LDH-Dye

The organic molecule PTPH is represented in Figure 2 a). It is composed of a pyrazino-1,3a,6a-triazapentalene molecular backbone with a 4-hexynoic acid substituent chain. Carboxylic acid group is attached to allow the intercalation of the dye molecules between the LDH sheets (Yan et al., 2014). The sample LDH-PTPH powder was synthetized by coprecipitation method. The XRD patterns of LDH-PTPH powder as well as pristine PTPH powder and reference LDH-NO_3 powder where nitrate anions are intercalated in a Zn_2Al LDH matrix, are represented in the Figure 3. Diffraction planes (00ℓ) are the fingerprints of the layered structure of LDH. For the reference sample LDH-NO_3, the positions of 2θ = 10.1° and 20.2° (i.e. 0.78 nm and 0.39 nm) are characteristic of a nitrate LDH phase and assigned to (003) and (006) diffraction planes, respectively (Mahjoubi et al., 2017). The basal spacing given by the Scherrer equation (Scherrer, 1912) is 0.78 nm for a (003) diffraction plan at a position of 2θ = 10.1°. (110) and (113) diffraction plans are partially overlapped around 2θ = 60.5° leading to a the metal-to-metal distance within the cationic hydroxide layers of a = $2d_{(110)}$= 3.1 Å, this in agreement with a ratio Zn : Al of 2 : 1 (Vial et al., 2006).

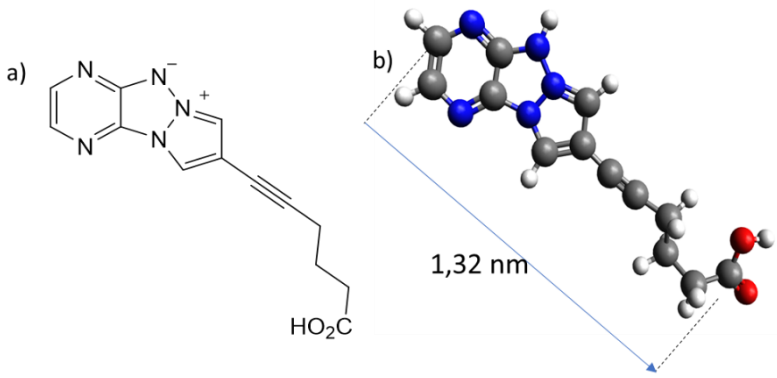
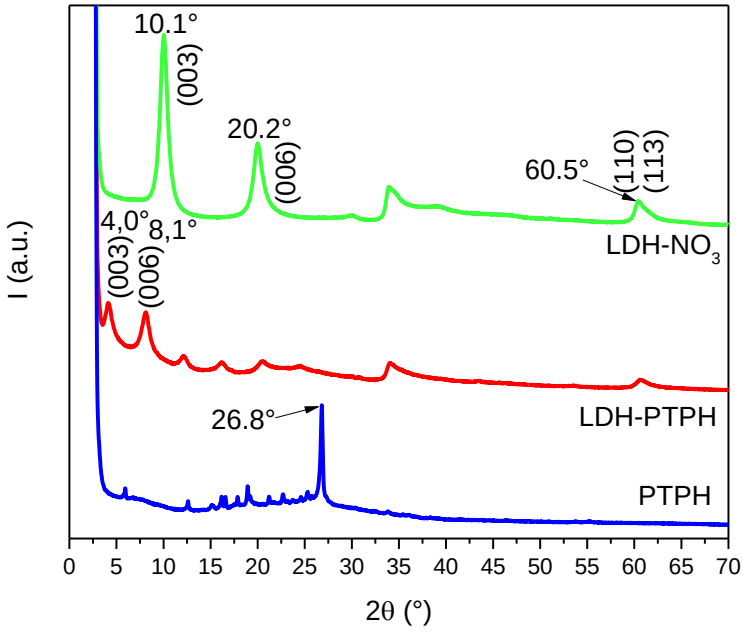


*Figure 2: a) Molecular structure of the studied dye: a pyrazino-1,3a,6a-triazapentalene type structure; b) 3D molecular structure of the dye **a** with calculated size of the molecule*

The diffraction plan (003) and (006) of the XRD pattern of LDH-PTPH are observed at lower 2θ, the peak positions are 4.0° and 8.1° meaning that the basal spacing (2.21 nm) is larger than for the LDH-NO_3 (I. Khan and O'Hare, 2002), thus indicating that the large molecules PTPH are intercalated into the LDH host. Moreover, the geometry of the dye was optimized with Avogadro software and the length of the molecule is estimated to be 1.32 nm (Figure 2 b)). The basal spacing agrees well the accommodation of the interleaved dye PTPH. The XRD pattern of the pristine sample PTPH is also represented, a narrow intense peak is observed at 2θ = 26.8° which is not observed for the XRD pattern of LDH-PTPH that excludes the structural packing of free PTPH molecules onto the sample. The mean crystallite size (L) was calculated according to the Scherrer equation $L = k\lambda/(B\cos\theta)$, where B is the full width at half maximum (FWHM) of the diffraction peak (003) and k is the shape factor of the average crystallite and fixed to k = 0.9 (assuming a spherical shape) (Cullity, 1978). A coherence length Lc along the stacking direction of 17 nm was found for the LDH-PTPH powder meaning that LDH aggregates are composed in average by less than ten stacked layers.



246

247 *Figure 3: X-Ray Diffractogram (XRD) of the pristine dye PTPH and intercalated in a Zn_2Al LDH matrix LDH-PTPH as well as a*
248 *reference Zn_2Al LDH matrix with nitrate anions intercalated: LDH-NO_3*

249 The FTIR spectra of PTPH and LDH-PTPH recorded between 400 and 4000 cm^{-1} (Figure 4).
250 Several characteristic bands are observed for the pristine powder PTPH at 1300 cm^{-1} (C-N
251 aromatic), 1515 cm^{-1} (C=C aromatic), 1715 cm^{-1} (stretching bond C=O from carboxylic acid)
252 and around 3100 cm^{-1} (C-H aromatic). These bands are also visible in the spectra of the LDH-
253 PTPH powder that confirms the presence of PTPH in the sample. However, the IR band at
254 1715 cm^{-1} (stretching bond C-O from carboxylic acid) disappears from the LDH-PTPH IR
255 spectra while a new band appears around 1560 cm^{-1} which is characteristic of stretching
256 bond C=O from carboxylate. Thus, XRD data as well as FTIR spectra confirm the intercalation
257 and its interaction, respectively, of the molecule PTPH under carboxylate form into the LDH
258 matrix.

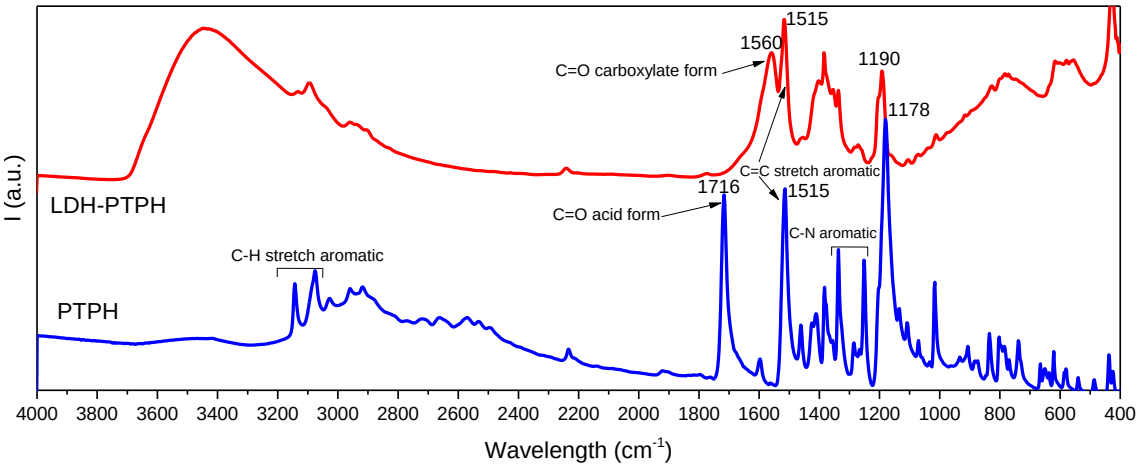


Figure 4: FTIR spectra of the pristine dye PTPH and intercalated in a Zn_2Al LDH matrix LDH-PTPH recorded into KBr pellets

The UV-Vis absorption spectra of PTPH and LDH-PTPH powders recorded into KBr pellets (Figure 5). Both powders present a large absorbance domain between 200 and 500 nm without a specific absorbance band. The intercalation of PTPH in the LDH matrix does not affect its own absorbance properties.

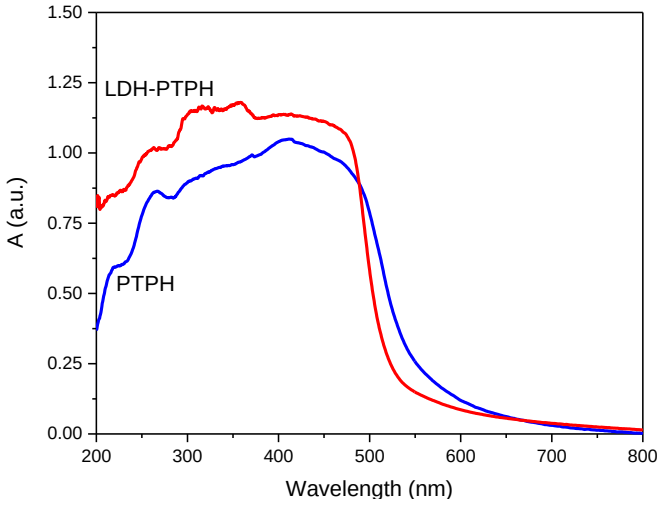


Figure 5: UV-visible spectra of the pristine dye PTPH and intercalated in a Zn2Al LDH matrix LDH-PTPH recorded into KBr pellets

3.2. Photoluminescence of the pristine dye and the LDH-Dye

The absolute PLQY of the dye recorded between 250 and 500 nm for the compound PTPH in aqueous solution and in dichloromethane solution at three concentrations (10^{-3}, 10^{-4} and 10^{-5} M) is displayed in Figure 6**.** Thanks to the carboxylate group and the polarity of the dye, PTPH is soluble in water. It is also soluble in organic polar solvent such as dichloromethane

or DMSO. The absolute PLQY of PTPH in water is silent; the quenching of luminescence properties occurs whatever the concentration. On the other hand, PTPH in dichloromethane exhibits high absolute PLQY. In a high diluted system (10^{-5} M), PTPH shows absolute PLQY between 340 and 465 nm, the absolute $PLQY_{max}$ is 20.3 % for λ_{exc} = 315 nm, whereas the absolute PLQY reaches 40.3 % for 10^{-4} M concentration. At 10^{-3} M, compound PTPH displays a saturation step between 370 and 450 nm due to high concentration.

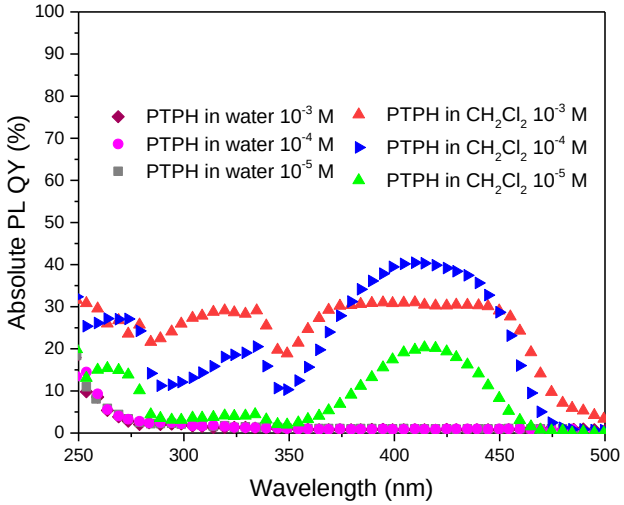


Figure 6: Absolute PLQY in function of the wavelength for solution of PTPH in water and in dichloromethane at three different concentration: 10^{-3}, 10^{-4} and 10^{-5} M

The absolute photoluminescence quantum yield (PLQY) of the pristine powder PTPH is illustrated on the Figure 7. The PLQY has been recorded between 250 and 500 nm as if the dye was associated with an UV-LED. The PLQY varies between 6 and 11 % and the maximum is reached at λ_{exc} = 315 nm. The values are weak for a potential lighting application but in fact they are very interesting for pristine solid organic dye. Indeed, most of the organic dyes at the solid state such as fluorescein or eosin do not present any luminescent properties at all.(De et al., 2005; De and Kundu, 2011; Yaguchi et al., 2012). The absolute PLQYs of LDH-PTPH under powder and paste form are also reported on the Figure 6. As reported in Experimental section, the paste is obtained after the washing/centrifugation process and before the drying process. The absolute PLQY of the LDH-PTPH powder is almost constant as

a function of the wavelength (around 2 %) and are much weaker than the absolute PLQY of the pristine powder PTPH**.** Expectedly, the dispersion of the dye into LDH matrix would allow to reproduce a solid state mixed into a solvated system as in a liquid solution to increase the absolute PLQY. However, the desired effect is not occurring as for the fluorescein(Legentil et al., 2019). The absolute PLQY of the LDH-PTPH paste is higher than the absolute PLQY of the powder, the absolute $PLQY_{max}$ is 11.9 % for λ_{exc} = 320 nm. Counter intuitively, the paste, which is just the powder dispersed in a small quantity of water, displays higher absolute PLQY than the powder, while the luminescence is quenched for PTPH dispersed in water.

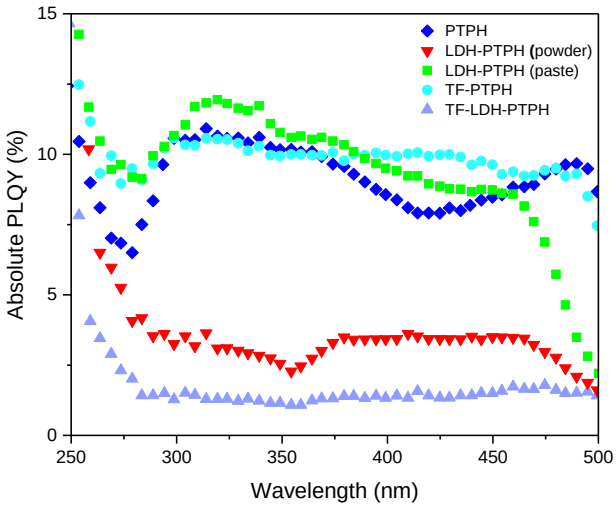


Figure 7: Absolute PLQY of powders PTPH and LDH- PTPH as well as paste LDH-PTPH and both composite thin films TF-PTPH and TF-LDH-PTPH

3.3. Characterisation of the thin film

Two composite thin films with a silicon matrix (PDMS) was prepared (Deng et al., 2016). The first one, TF-PTPH**,** was prepared with pristine powder PTPH with a loading rate of 5 wt. % whereas the second one, TF-LDH-PTPH, was elaborated with the LDH-PTPH powder with a loading rate of 20 $\%_w$ to get around 5 $\%_w$ of PTPH. Both films under UV radiation and under daylight are illustrated in the Figure 8. First of all, one may observe that the dispersion of PTPH molecule in the polymer matrix is quite inhomogeneous, as small aggregates are visible in the thin film TF-PTPH leading to a granular aspect. On the contrary, the dispersion in TF-

LDH-PTPH is homogeneous without any aggregates. Thus, LDH matrix has a real additional value in dispersing of the dye PTPH into a polymer matrix. However, TF-PTPH seems to be more luminescent than TF-LDH-PTPH under UV radiation where luminescence is completely turned-off.

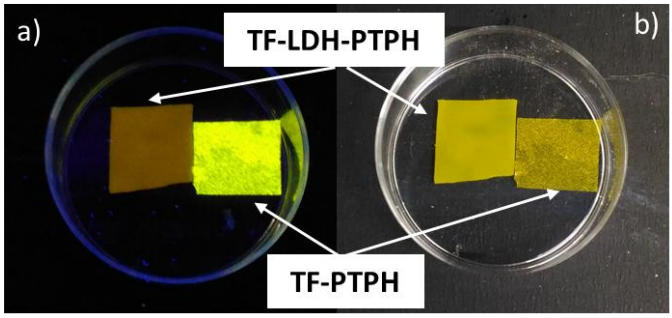


Figure 8: Composite thin films of TF-LDH-PTPH and TF-PTPH under daylight and UV irradiation (λ=265 nm)

The FTIR spectra of LDH-PTPH and TF-LDH-PTPH recorded between 400 and 4000 cm^{-1} (Figure 9). For TF-LDH-PTPH, several IR bands can be attributed to the PDMS polymer (2880-2960, 2140, 1945, 1445, 1415 cm^{-1}) (Bodas and Khan-Malek, 2006). Only two bands, relating to compound PTPH, at 1515 et 1560 cm^{-1} are observed. Thus, the dispersion in the matrix polymer does not modify or degrade the LDH-PTPH powder.

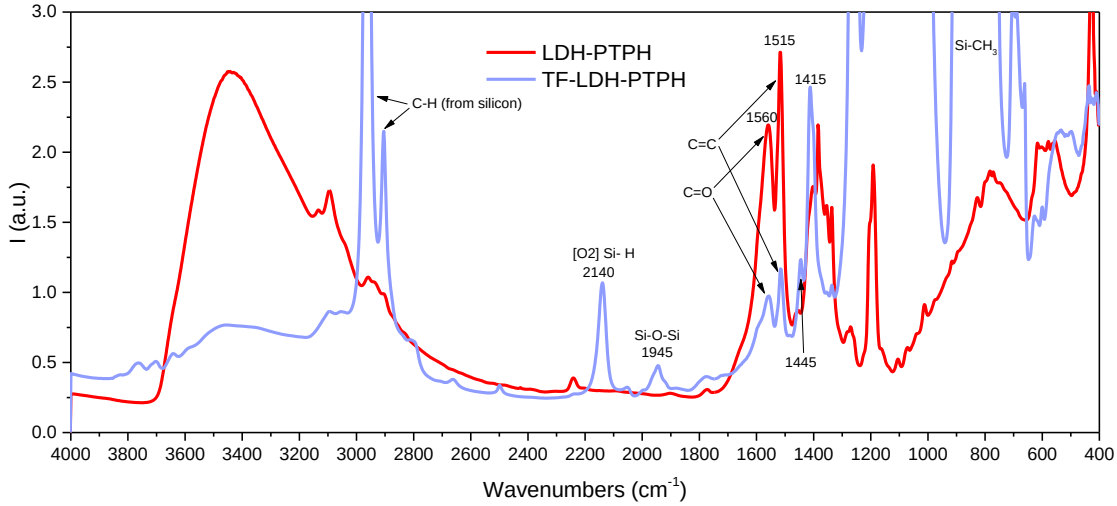


Figure 9: FTIR spectra of powder LDH-PTPH recorded into KBr pellets and the composite thin film TF-LDH-PTPH between 400 and 4000 cm^{-1}

The small-angle X-ray scattering data of both composite films TF-LDH-PTPH and reference silicon film are presented in Figure 10. Scattered intensity I is plotted versus the scatter vector q, where $q = 4\pi\sin(\theta)/\lambda$. For TF-LDH-PTPH, a characteristic LDH pattern is observed (Schaefer and Justice, 2007; Seftel et al., 2015). Two diffraction peaks are observed at 0.26 and 0.53 $Å^{-1}$ corresponding to distances of 2.42 and 1.18 nm, the first one is the basal spacing of the LDH matrix. For PEO-HDL-PTPH, only one diffraction peak is observed at 0.33 $Å^{-1}$ corresponding to a basal spacing of 1.90 nm. These values are closed and match with data obtained from X-ray diffractogram of the powder LDH-PTPH (2.21 nm). According with other SAXS investigations (Jarzębski et al., 1997; Tokudome et al., 2016; Wu et al., 2007), the mean size (L) of secondary aggregated particles, i.e. LDH pellets, can be calculated from the scatter vector found between the slop modifications of the curve. L_2 = 27.3 nm and L_1 = 23.1 nm were measured, respectively for TF-LDH-PTPH and for PEO-HDL-PTPH. These values are slightly higher than the size (Lc = 17 nm) obtained through the Scherrer equation from the X-ray diffractogram of the powder HDL-PTPH. It could be explained by a modification of the environment into the basal spacing or a swelling effect due to the polymer matrices.

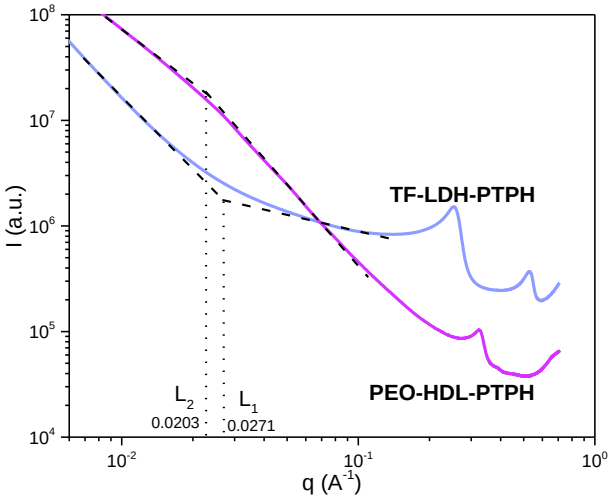


Figure 10: Small-angle X Ray scattering (SAXS) of thin composite film TF-LDH-PTPH and a reference silicone film

3.4. Photoluminescence of the thin film

The absolute PLQY of both composite films TF-LDH-PTPH and TF-PTPH are presented on Figure 7. The PLQY of TF-PTPH are close to those of the pristine powder PTPH with a maximum of 11 % for λ_{exc} = 315 nm. The PLQY of the composite film TF-LDH-PTPH is extremely weak, between 1 and 2 %. The luminescence of the thin film is barely observed under UV irradiation. These results show that the intercalation of the molecule PTPH into LDH host is not suitable for the luminescence properties, this is also the case after dispersion into a PDMS-type polymer.

A hydrophilic polymer PEO is then used to prepare a second composite film with the LDH-PTPH paste which presents decent photoluminescence property. The absolute PLQY of the film PEO-LDH-PTPH were presented on Figure 11. The PLQY between 250 and 500 nm are perfectly matching with the PLQY of LDH-PTPH paste. The photoluminescence property of the paste is preserved through its dispersion into a hydrophilic polymer such as PEO, then yielding a luminescent composite film. Further studies are needed to unravel the unexpected behaviour of the observed stable luminescence in such medium.

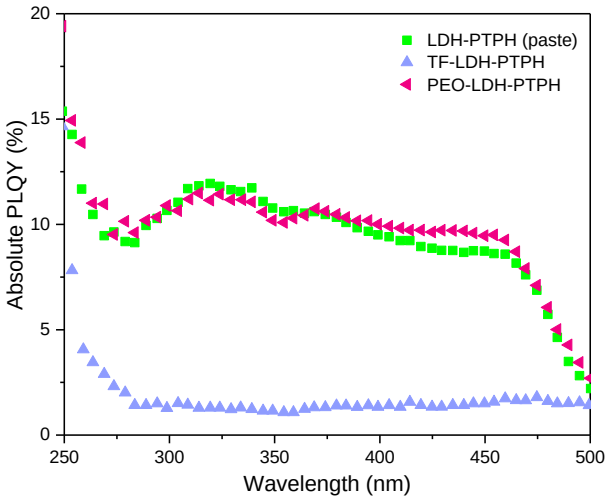


Figure 11: Absolute PLQY of composite films PEO-LDH-PTPH and TF-LDH-PTPH as well as paste LDH-PTPH

4. Conclusion

The study demonstrates that the organic molecule PTPH (pyrazino-1,3a,6a-triazapentalene type structure) exhibits efficient photoluminescence property for an organic molecule at solid state. The cumbersome organic guest PTPH is well intercalated into LDH matrix Zn_2Al using a coprecipitation method, enough ensconced to get a hybrid luminescent material. Counter intuitively, the LDH-PTPH powder does not emit any radiation under blue/UV excitation (absolute PLQY lower than 2 %) whereas the LDH-PTPH paste produces luminescence with an absolute $PLQY_{max}$ of 11.9 % for λ_{exc} = 320 nm. The dispersion of the LDH-PTPH powder in a polymer (PDMS) occurs readily thanks to the compatible LDH host matrix. However, such dispersion is not able to produce luminescence enough. When hydrophilic polymer such as poly(ethylene oxide) is combined with the LDH-PTPH paste, the absolute PLQY is similar to LDH-PTPH paste values, reaching an absolute $PLQY_{max}$ of 11.5 % for λ_{exc} = 315 nm, and showing that the continuous phase; i.e. polymer, may play a role at nanoscale.

Acknowledgement

This work was supported by CPER DEFI MMASYF through its 2016 «MetaProfile» project. Thus, the authors thank European Union in the framework of the European Regional Development Fund (ERDF), and Région Auvergne Rhône-Alpes for the SAXS equipment acquisition and P.L. for his PhD funding « CPER ». In addition, this work was partially supported by Labex SynOrg (ANR-11-LABX-0029), University of Orléans and Région Centre Val de Loire (S2E2 certified OrgaLight project).

References

Almasian, A., Mirjalili, M., Maleknia, L., Giahi, M., 2019. Preparation of Multi-Functional Polyester Fabrics with the Use of a New Organo-Clay Nanopigment in High Temperature/High Pressure Condition. Fibers and Polymers 20, 1387-1395.

Aloisi, G.G., Costantino, U., Elisei, F., Latterini, L., Natali, C., Nocchetti, M., 2002. Preparation and photo-physical characterisation of nanocomposites obtained by intercalation and co-intercalation of organic chromophores into hydrotalcite-like compounds. Journal of Materials Chemistry 12, 3316-3323.

Bodas, D., Khan-Malek, C., 2006. Formation of more stable hydrophilic surfaces of PDMS by plasma and chemical treatments. Microelectronic Engineering 83, 1277-1279.

Costantino, U., Coletti, N., Nocchetti, M., Aloisi, G.G., Elisei, F., 1999. Anion Exchange of Methyl Orange into Zn−Al Synthetic Hydrotalcite and Photophysical Characterization of the Intercalates Obtained. Langmuir 15, 4454-4460.

Costantino, U., Coletti, N., Nocchetti, M., Aloisi, G.G., Elisei, F., Latterini, L., 2000. Surface Uptake and Intercalation of Fluorescein Anions into Zn−Al−Hydrotalcite. Photophysical Characterization of Materials Obtained. Langmuir 16, 10351-10358.

Costantino, U., Costantino, F., Elisei, F., Latterini, L., Nocchetti, M., 2013. Coupling physical chemical techniques with hydrotalcite-like compounds to exploit their structural features and new multifunctional hybrids with luminescent properties. Physical Chemistry Chemical Physics 15, 13254-13269.

Cullity, B.D., 1978. Elements of X-ray Diffraction. Addison-Wesley Publishing Company.

Davis, R., Saleesh Kumar, N.S., Abraham, S., Suresh, C.H., Rath, N.P., Tamaoki, N., Das, S., 2008. Molecular Packing and Solid-State Fluorescence of Alkoxy-Cyano Substituted Diphenylbutadienes: Structure of the Luminescent Aggregates. The Journal of Physical Chemistry C 112, 2137-2146.

De, S., Das, S., Girigoswami, A., 2005. Environmental effects on the aggregation of some xanthene dyes used in lasers. Spectrochimica Acta Part A: Molecular and Biomolecular Spectroscopy 61, 1821-1833.

De, S., Kundu, R., 2011. Spectroscopic studies with fluorescein dye—Protonation, aggregation and interaction with nanoparticles. Journal of Photochemistry and Photobiology A: Chemistry 223, 71-81.

Deng, S., Binauld, S., Mangiante, G., Frances, J.M., Charlot, A., Bernard, J., Zhou, X., Fleury, E., 2016. Microcrystalline cellulose as reinforcing agent in silicone elastomers. Carbohydrate Polymers 151, 899-906.

Dou, Y., Liu, X., Shao, M., Han, J., Wei, M., 2013. Flexible and transparent free-standing films with enhanced magnetic and luminescent anisotropy. Journal of Materials Chemistry A 1, 4786-4792.

Gogoi, B., Sen Sarma, N., 2015. Curcumin-cysteine and curcumin-tryptophan conjugate as fluorescence turn on sensors for picric Acid in aqueous media. ACS applied materials & interfaces 7, 11195-11202.

Hajibeygi, M., Omidi-Ghallemohamadi, M., 2017. One-step synthesized azo-dye modified Mg-Al LDH reinforced biobased semi-aromatic polyamide containing naphthalene ring; study on thermal stability and optical properties. Journal of Polymer Research 24, 61.

I. Khan, A., O'Hare, D., 2002. Intercalation Chemistry of Layered Double Hydroxides: Recent Developments and Applications.

Jarzębski, A.B., Lorenc, J., Pająk, L., 1997. Surface Fractal Characteristics of Silica Aerogels. Langmuir 13, 1280-1285.

Kumar, S., Singh, P., Srivastava, R., Koner, R., Pramanik, A., Mathew, J., Sinha, S., Rawat, M., Anand, R., Ghosh, S., 2014. Engineering Fused Coumarin Dyes: Molecular Level Understanding of Aggregation Quenching and Tuning Electroluminescence via Alkyl Chain Substitution.

Latterini, L., Elisei, F., Aloisi, G.G., Costantino, U., Nocchetti, M., 2002. Space-resolved fluorescence properties of phenolphthalein-hydrotalcite nanocomposites. Physical Chemistry Chemical Physics 4, 2792-2798.

Legentil, P., Leroux, F., Therias, S., Mahiou, R., Chadeyron, G., 2019. Revisiting fluorescein and layered double hydroxide using a synergistic approach: A complete optical study. Journal of Luminescence 215, 116634.
Lu, T.-F., Li, W., Zhang, H.-X., 2018. Rational design of metal-free organic D-π-A dyes in dye-sensitized solar cells: Insight from density functional theory (DFT) and time-dependent DFT (TD-DFT) investigations. Organic Electronics 59, 131-139.
Mahajan, P.G., Dige, N.C., Vanjare, B.D., Eo, S.-H., Kim, S.J., Lee, K.H., 2019. A nano sensor for sensitive and selective detection of Cu2+ based on fluorescein: Cell imaging and drinking water analysis. Spectrochimica Acta Part A: Molecular and Biomolecular Spectroscopy 216, 105-116.
Mahjoubi, F.Z., Khalidi, A., Abdennouri, M., Barka, N., 2017. Zn–Al layered double hydroxides intercalated with carbonate, nitrate, chloride and sulphate ions: Synthesis, characterisation and dye removal properties. Journal of Taibah University for Science 11, 90-100.
Marangoni, R., Taviot-Guého, C., Illaik, A., Wypych, F., Leroux, F., 2008. Organic inorganic dye filler for polymer: Blue-coloured layered double hydroxides into polystyrene. Journal of Colloid and Interface Science 326, 366-373.
Math, N.N., Naik, L.R., Suresh, H.M., Inamdar, S.R., 2006. Dual fluorescence and laser emissions from fluorescein-Na and eosin-B. Journal of Luminescence 121, 475-487.
Mekhzoum, M.E.M., Essassi, E.M., Qaiss, A., Bouhfid, R., 2016. Fluorescent bio-nanocomposites based on chitosan reinforced hemicyanine dye-modified montmorillonite. RSC Advances 6, 111472-111481.
Saha, M., Shil, A., Hussain, S.A., Bhattacharjee, D., 2017. Clay induced changes in the aggregation pattern of Safranine-O in hybrid Langmuir-Blogdgett (LB) films. Journal of Photochemistry and Photobiology A: Chemistry 348, 199-208.
Schaefer, D.W., Justice, R.S., 2007. How Nano Are Nanocomposites? Macromolecules 40, 8501-8517.
Scherrer, P., 1912. Bestimmung der inneren Struktur und der Größe von Kolloidteilchen mittels Röntgenstrahlen, Kolloidchemie Ein Lehrbuch. Springer Berlin Heidelberg, Berlin, Heidelberg, pp. 387-409.
Schoonheydt, R., Johnston, C.T., Bergaya, F., 2018. Surface and interface chemistry of clay minerals.
Seftel, E., Niarchos, M., Vordos, N., Nolan, J., Mertens, M., Mitropoulos, A.C., Vansant, E., Cool, P., 2015. LDH and TiO2/LDH-type nanocomposite systems: A systematic study on structural characteristics.
Sen, T.K., 2017. Clay minerals : properties, occurrence, and uses. Nova Science Publishers.
Shi, W., Sun, Z., Wei, M., Evans, D.G., Duan, X., 2010. Tunable Photoluminescence Properties of Fluorescein in a Layered Double Hydroxide Matrix by Changing the Interlayer Microenvironment. The Journal of Physical Chemistry C 114, 21070-21076.
Sirbu, D., Diharce, J., Martinić, I., Chopin, N., Eliseeva, S.V., Guillaumet, G., Petoud, S., Bonnet, P., Suzenet, F., 2019. An original class of small sized molecules as versatile fluorescent probes for cellular imaging. Chemical communications 55, 7776-7779.
Tokudome, Y., Morimoto, T., Tarutani, N., Vaz, P.D., Nunes, C.D., Prevot, V., Stenning, G.B.G., Takahashi, M., 2016. Layered Double Hydroxide Nanoclusters: Aqueous, Concentrated, Stable, and Catalytically Active Colloids toward Green Chemistry. ACS Nano 10, 5550-5559.
Vial, S., Ghanbaja, J., Forano, C., 2006. Precipitation of Zn2Al LDH by urease enzyme. Chemical communications, 290-292.
Volpi, G., Lace, B., Garino, C., Priola, E., Artuso, E., Cerreia Vioglio, P., Barolo, C., Fin, A., Genre, A., Prandi, C., 2018. New substituted imidazo[1,5-a]pyridine and imidazo[5,1-a]isoquinoline derivatives and their application in fluorescence cell imaging. Dyes and Pigments 157, 298-304.
Weber, M.D., Niklaus, L., Proschel, M., Coto, P.B., Sonnewald, U., Costa, R.D., 2015. Bioinspired Hybrid White Light-Emitting Diodes. Advanced materials 27, 5493-5498.
Wu, H., Huang, Z., Hua, T., Liao, C., Meier, H., Tang, H., Wang, L., Cao, D., 2019. Metal-free organic dyes with di(1-benzothieno)[3,2-b:2′,3′-d]pyrrole as a donor for efficient dye-sensitized solar cells: Effect of mono- and bi-anchors on photovoltaic performance. Dyes and Pigments 165, 103-111.

Wu, Q., Sjåstad, A.O., Vistad, Ø.B., Knudsen, K.D., Roots, J., Pedersen, J.S., Norby, P., 2007. Characterization of exfoliated layered double hydroxide (LDH, Mg/Al = 3) nanosheets at high concentrations in formamide. Journal of Materials Chemistry 17, 965-971.

Yaguchi, K., Furube, A., Katoh, R., 2012. Aggregate formation of eosin-Y adsorbed on nanocrystalline TiO2 films. Chemical Physics Letters 551, 96-100.

Yan, D., Lu, J., Wei, M., Qin, S., Chen, L., Zhang, S., Evans, D.G., Duan, X., 2011. Heterogeneous Transparent Ultrathin Films with Tunable-Color Luminescence Based on the Assembly of Photoactive Organic Molecules and Layered Double Hydroxides. Advanced Functional Materials 21, 2497-2505.

Yan, L., Wang, Y., Li, J., Kalytchuk, S., Susha, A.S., Kershaw, S.V., Yan, F., Rogach, A.L., Chen, X., 2014. Highly luminescent covalently bonded layered double hydroxide–fluorescent dye nanohybrids. Journal of Materials Chemistry C 2, 4490.

Zhang, L., Li, B., Lei, B., Hong, Z., Li, W., 2008. A triphenylamine derivative as an efficient organic light color-conversion material for white LEDs. Journal of Luminescence 128, 67-73.

Supporting information

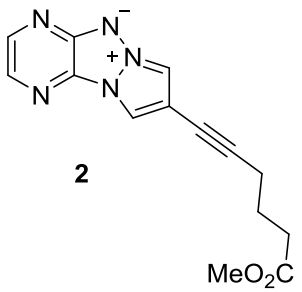
Materials and methods

Nuclear Magnetic Resonance (NMR) spectra were recorded on a 250 or 400 MHz Bruker NMR spectrometers in $CDCl_3$ or DMSO. All chemical shift values are reported in parts per million (ppm) with coupling constant (J) values reported in Hz. All spectra were referenced to the $CDCl_3$ residual solvent peak $CHCl_3$ (δ = 7.26 ppm) for ^{1}H NMR and the $CDCl_3$ solvent peak (δ = 77.16 ppm) for ^{13}C NMR. The notation of signals is: Proton: δ chemical shift in ppm (multiplicity, J value(s), number of protons). Carbon: δ chemical shift in ppm. Fluorine: δ chemical shift in ppm. Splitting patterns are assigned s = singlet, b = broad, d = doublet, td = triplet of doublet, dt = doublet of triplet, t = triplet, q = quartet, app= apparent.

All reaction were monitored by thin-layer chromatography (TLC) analysis using silica gel (60 F254). Solvents, unless otherwise stated, were purchased in reagent grade or anhydrous quality and used as received. Reagents were either purchased directly from commercial suppliers or prepared according to literature procedures. Yields of all the compounds refer to isolated compounds. Chromatography: Separations were carried out on Silica gel 60, (40-63 μ, 60 Å) purchased from Sigma Aldrich. High Resolution Mass Spectrometry (HRMS) were recorded on Maxis Bruker 4G. Melting points (mp [C°]) were taken on open capillary tubes using a Electrothermal IA 9100 apparatus.

Reactants were purchased from commercial suppliers and were used without further purification. Compound **1** was synthesized following reported synthesis (Sirbu et al., 2019).

Experimental procedures



In a round bottom flask, the bromopyridazinotriazapentalene **1** (Sirbu et al., 2019) (1.0 g, 4.20 mmol) was solubilized in Et_3N (10 mL) with methyl-5-hexynoate (1.060 g, 8.40 mmol, 2 eq.) and $Pd(PPh_3)_2Cl_2$ (294.8 mg, 0.42 mmol, 10 mol%). The mixture was stirred at room temperature for 20 min and then CuI (72.4 mg, 0.38 mmol, 9 mol%) was added. The mixture was stirred at 90°C for 3h. Solvent was removed under vaccum and crude compound purified by column chromatography (DCM/AcOEt 1/1) to give pure **2** (900 mg, 76%) as a yellow solid.

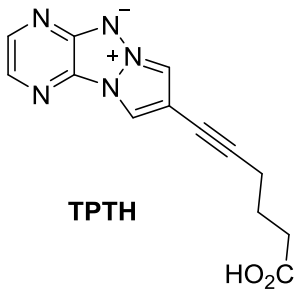
P*f* : 99°C

IR $\nu(cm^{-1})$: 3138, 3078, 2959, 1721, 1507, 1424, 1382, 1368, 1336, 1256, 1186.

^{1}H NMR (400 MHz, Chloroform-d) δ 8.35 (d, *J* = 2.7 Hz, 1H), 8.03 (s, 1H), 7.83 (d, *J* = 2.7 Hz, 1H), 7.78 (s, 1H), 3.63 (s, 3H), 2.45 (td, *J* = 7.2, 5.4 Hz, 4H), 1.89 (p, *J* = 7.2 Hz, 2H).

^{13}C NMR (101 MHz, $CDCl_3$) δ 173.27, 152.43, 143.33, 130.43, 128.94, 111.86, 110.52, 107.83, 93.28, 70.19, 51.66, 32.81, 23.49, 18.86.

HRMS (ESI) *m/z* : calculated for $C_{14}H_{14}N_5O_2$ $[M+H]^+$ 284.1142 ; found 284.1141.



TPTH

In a round bottom flask, **2** (500 mg, 1.77 mmol) was solubilized in MeOH (4 mL) with NaOH 10N (1 mL, 10 mmol, 5.6 eq.). The mixture was stirred at room temperature for 2h. Solvents were removed under vaccum and the crude mixture solubilized in DCM and water (1/1). Aqueous phase was extracted and washed with DCM (3 x 20 mL) and then acidified with HCl 2N until pH 4-5. Organic phase was extracted with DCM, washed with water and concentrated under vacuo to give pure **TPTH** (377 mg, 1.40 mmol, 79%).

P*f* : ~175°C (decomp.)

IR ν(cm^{-1}) : 3143, 3074, 2960, 1715, 1512, 1382, 1336, 1250, 1176, 1016.

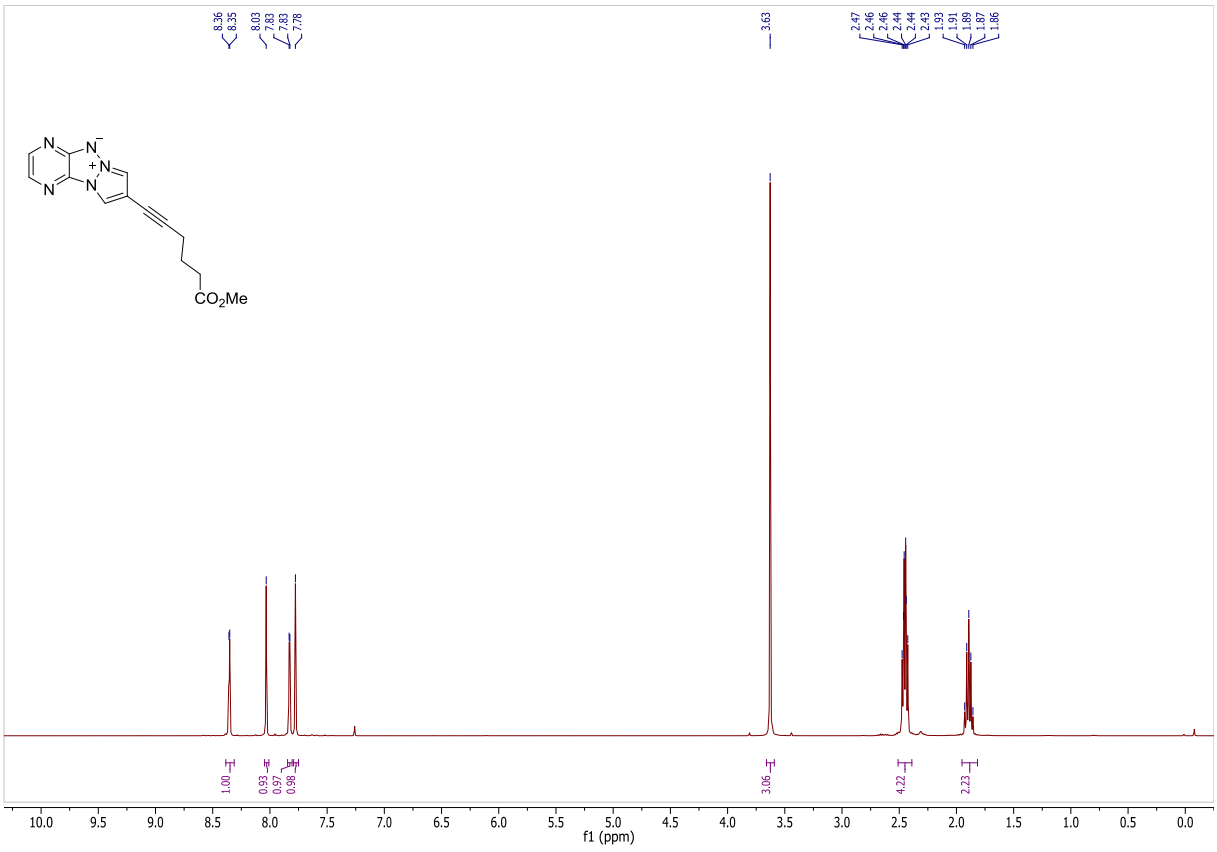
^{1}H NMR (400 MHz, DMSO-d6) δ 12.14 (s, 1H), 8.85 (s, 1H), 8.58 (s, 1H), 8.36 (d, *J* = 2.7 Hz, 1H), 7.90 (d, *J* = 2.7 Hz, 1H), 2.55 – 2.46 (m, 2H), 2.38 (t, *J* = 7.3 Hz, 2H), 1.78 (p, *J* = 7.2 Hz, 2H).

^{13}C NMR (101 MHz, DMSO) δ 173.96, 152.08, 142.65, 129.59, 128.92, 113.90, 111.37, 106.68, 92.99, 70.80, 32.60, 23.46, 18.16.

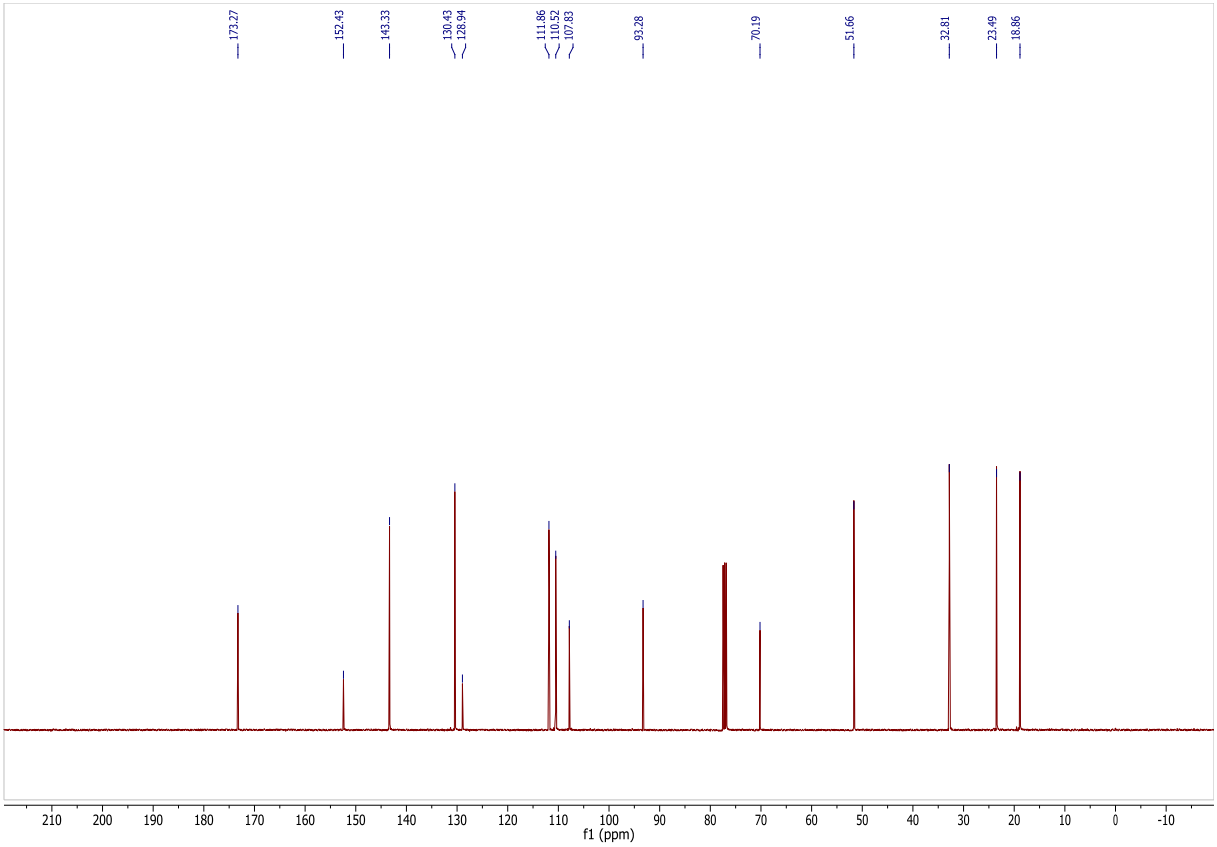
HRMS (ESI) *m/z* : calculated for $C_{13}H_{12}N_5O_2$ $[M+H]^+$ 270.0985; found 270.0984.

559

560 **NMR spectra**

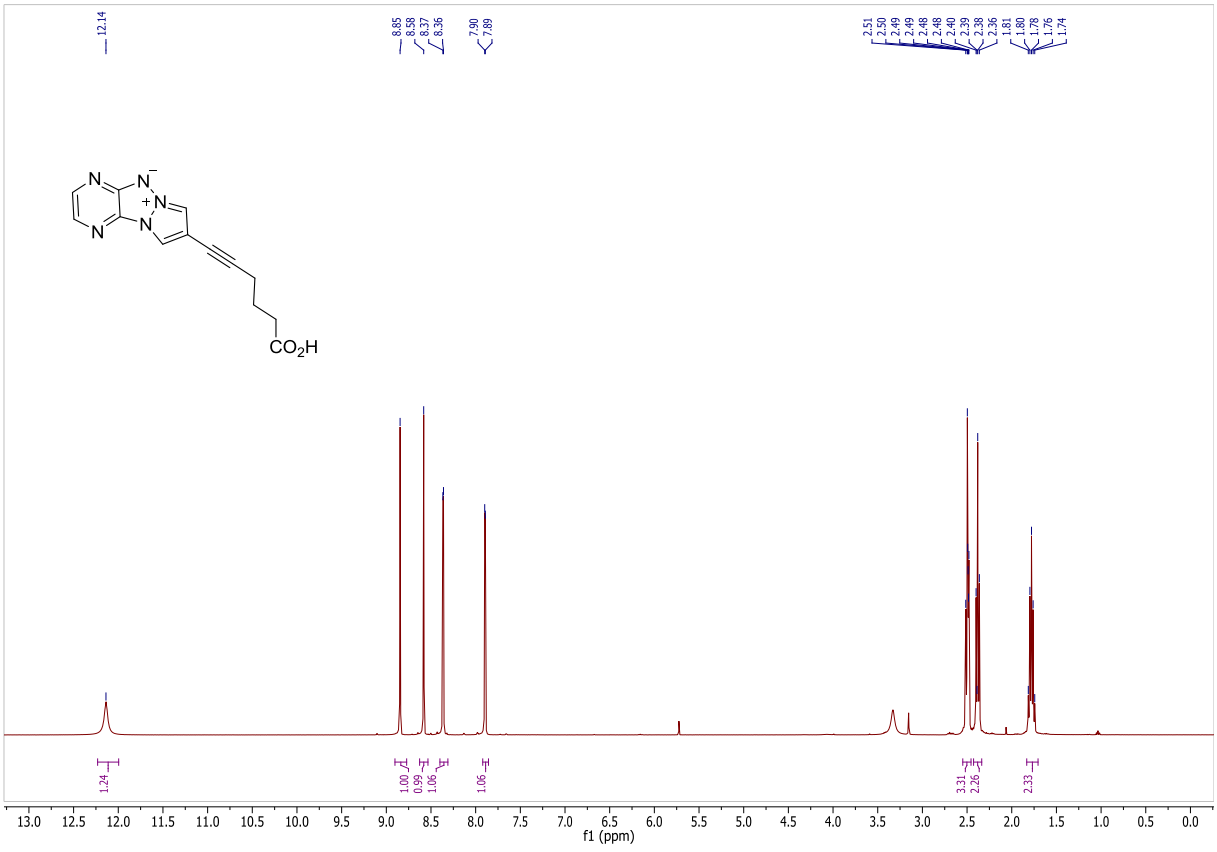


561

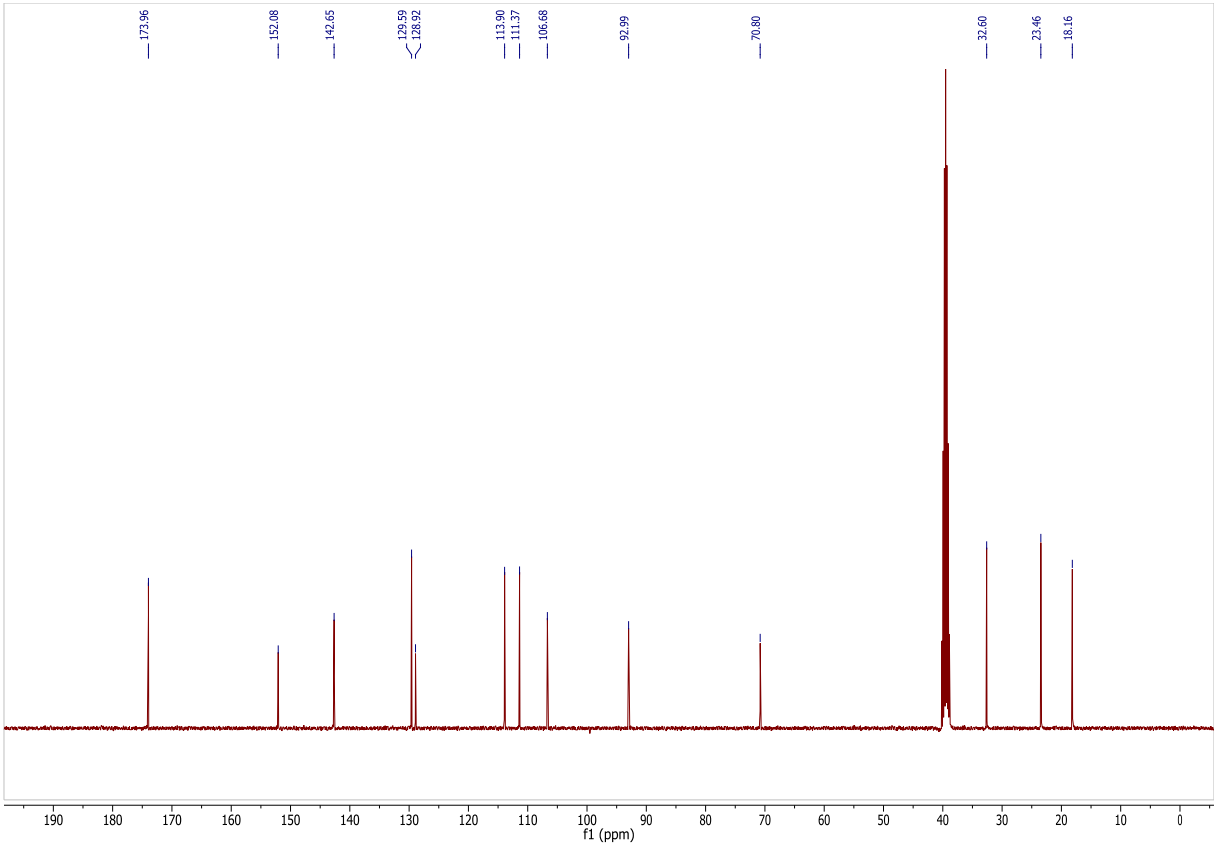

173.27
152.43
143.33
130.43
128.94
111.86
110.52
107.83
93.28
70.19
51.66
32.81
23.49
18.86
f1 (ppm)

562

563


12.14
8.85
8.58
8.37
8.36
7.90
7.89
2.51
2.50
2.49
2.49
2.48
2.48
2.40
2.39
2.38
2.36
1.81
1.80
1.78
1.76
1.74
CO2H
1.24
1.00
0.99
1.06
1.06
3.31
2.26
2.33
f1 (ppm)

564


173.96
152.08
142.65
129.59
128.92
113.90
111.37
106.68
92.99
70.80
32.60
23.46
18.16
190
180
170
160
150
140
130
120
110
100
90
80
70
60
50
40
30
20
10
0
f1 (ppm)

565